SCT-09, 2-7 August 2009, Chernogolovka

Two different kinds of rogue waves in weakly crossing sea states

Victor P. Ruban

Landau Institute for Theoretical Physics RAS

Formation of giant waves in sea states with two spectral maxima, centered at close wave vectors $\mathbf{k}_0 \pm \Delta\mathbf{k}/2$ in the Fourier plane, is numerically simulated using the fully nonlinear model for long-crested water waves [V. P. Ruban, Phys. Rev. E **71**, 055303(R) (2005)]. Depending on an angle θ between the vectors $\mathbf{k}_0$ and $\Delta\mathbf{k}$, which determines a typical orientation of interference stripes in the physical plane, rogue waves arise having different spatial structure. If $\theta \lesssim \arctan(1/\sqrt{2})$, then typical giant waves are relatively long fragments of essentially two-dimensional (2D) ridges, separated by wide valleys and consisting of alternating oblique crests and troughs. At nearly perpendicular $\mathbf{k}_0$ and $\Delta\mathbf{k}$, the interference minima develop to coherent structures similar to the dark solitons of the nonlinear Schrodinger equation, and a 2D freak wave looks much as a piece of a 1D freak wave, bounded in the transversal direction by two such dark solitons.

V. P. Ruban, Phys. Rev. E. **79**, 065304(R) (2009).

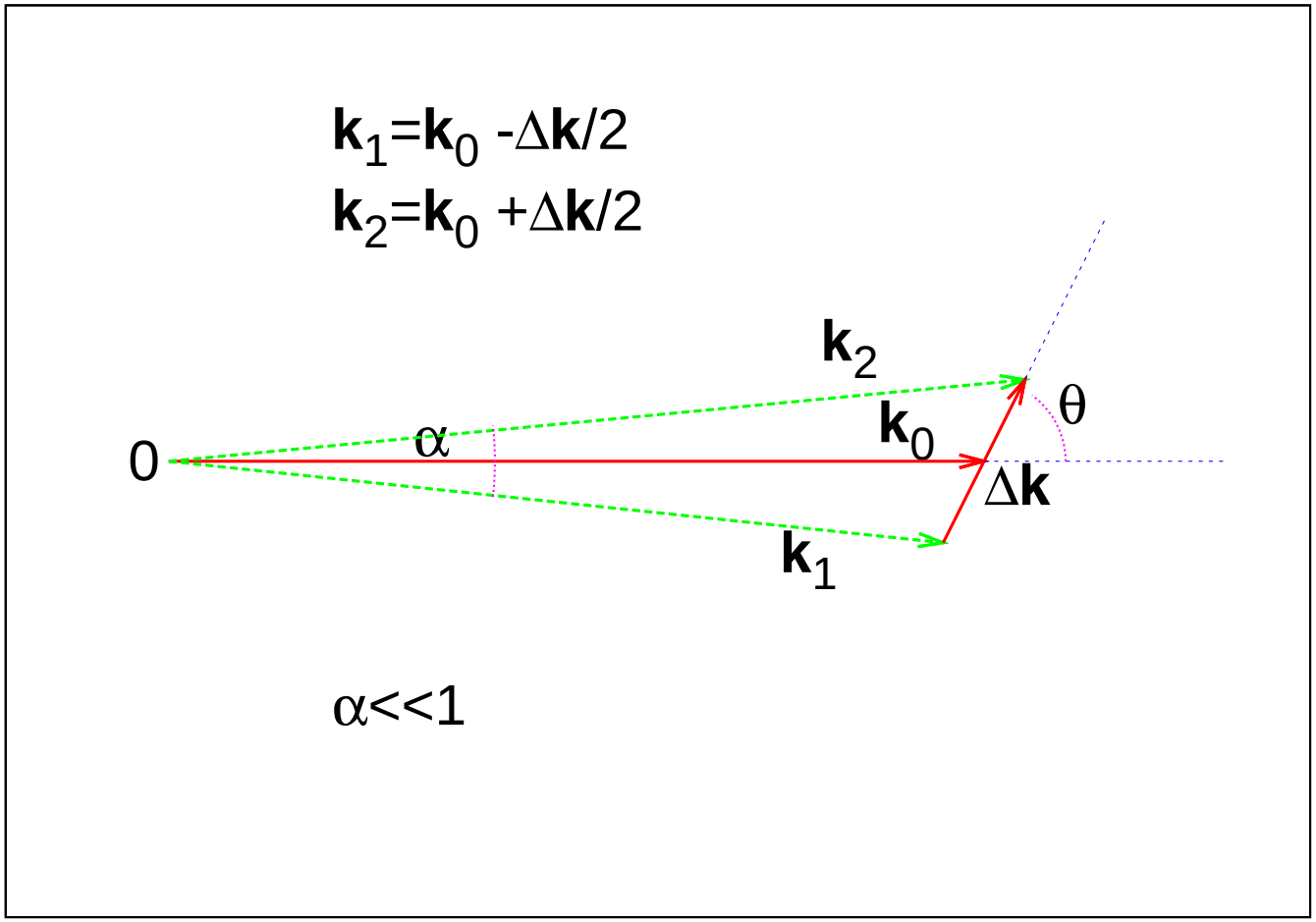

Figure 1: Two spectral maxima are assumed to be at wave vectors $\mathbf{k}_1$ and $\mathbf{k}_2$ in the Fourier plane.

I. Preliminary qualitative remarks

Weakly nonlinear deep-water gravity waves: 2D NLSE for wave envelope

$$Y(x_1, x_2, t) \approx \mathrm{Re}\left[A(x_1, x_2, t)\exp(ik_0x_1 - i\omega_0 t)\right], \tag{1}$$

$$\frac{i}{\omega_0}\frac{\partial A}{\partial t} + \frac{i}{2k_0}\frac{\partial A}{\partial x_1} = \frac{1}{8k_0^2}\left(\frac{\partial^2 A}{\partial x_1^2} - 2\frac{\partial^2 A}{\partial x_2^2}\right) + \frac{k_0^2}{2}|A|^2 A. \tag{2}$$

Simple 1D-reductions

$$A = k_0^{-1}\Psi(\xi, \tau) \tag{3}$$

$$\xi = k_0[(x_1 - V_{\mathrm{gr}}t)\cos\theta + x_2\sin\theta], \quad \tau = \omega_0 t, \quad V_{\mathrm{gr}} = (\omega_0/2k_0). \tag{4}$$

$$i\Psi_\tau = \frac{1}{4}\left[(1/2)\cos^2\theta - \sin^2\theta\right]\Psi_{\xi\xi} + \frac{1}{2}|\Psi|^2\Psi. \tag{5}$$

Depending on the sign of the dispersion coefficient $D(\theta) = [(1/2)\cos^2\theta - 2\sin^2\theta]$, the dynamics is quite different. For example, in the focusing case (when $D > 0$), the nonlinearity can become saturated with the so-called (bright) solitons,

$$\Psi_{\rm bs} = \frac{s}{\cosh\left[(s/\sqrt{D})(\xi - \xi_0)\right]} \exp(-i\tau s^2/4 + i\phi_0), \qquad (6)$$

where s is a wave steepness, and ξ_0, ϕ_0 are arbitrary constants. These weakly nonlinear solutions describe infinitely long wave ridges consisting of alternating oblique crests and troughs. In a more accurate model for fully nonlinear long-crested deep-water waves, as discussed below, these solutions exist for a long time, before qualitative modifications, in a range $0 < s \lesssim 0.24...0.27$ (depending on θ). In particular, if $\theta = 0$, in the highly nonlinear case $s = 0.20...0.27$ we have here the so called 1D GIANT BREATHERS (Dyachenko, Zakharov).

In the defocusing case (when $D < 0$), the so-called dark solitons are possible,

$$\Psi_{\rm ds} = s\tanh\left[(s/\sqrt{-D})(\xi - \xi_0)\right] \exp(-i\tau s^2/2 + i\phi_0), \qquad (7)$$

which separate two domains of opposite amplitude.

In view of the above, it is clear that since the effective dispersion coefficient $D(\theta)$ changes the sign at $\theta_* = \arctan(1/\sqrt{2})$, in the full 2D dynamics of random wave fields there should be two substantially different regimes, one regime at $\theta \lesssim \theta_*$ and another at θ close to $\pi/2$. This hypothesis is confirmed in general by numerical experiments reported here.

II. More accurate model

1. Conformal variables in 3D

$$Z = X + iY = z(u,q,t) = u + (i - \hat{H})Y(u,q,t) \tag{8}$$

$$\hat{H}Y(u,q,t) = \int [i\,\mathsf{sign}\,k]Y_{km}(t)e^{iku+imq}dk\,dm/(2\pi)^2 \tag{9}$$

$$Z_t = iZ_u(1 + i\hat{H})\left[\frac{(\delta\mathcal{K}/\delta\psi)}{|Z_u|^2}\right], \tag{10}$$

$$\begin{aligned}\psi_t \;=\; & -g\,\mathsf{Im}\,Z - \psi_u\hat{H}\left[\frac{(\delta\mathcal{K}/\delta\psi)}{|Z_u|^2}\right] \\ & + \frac{\mathsf{Im}\left((1 - i\hat{H})\left[2(\delta\mathcal{K}/\delta Z)Z_u + (\delta\mathcal{K}/\delta\psi)\psi_u\right]\right)}{|Z_u|^2}.\end{aligned} \tag{11}$$

2. Approximate kinetic energy functional

$$\mathcal{K} \approx \tilde{\mathcal{K}} = -\frac{1}{2}\int \psi \hat{H}\psi_u \, du\, dq + \tilde{\mathcal{F}}, \tag{12}$$

$$\begin{aligned}\tilde{\mathcal{F}} \;=\; & \frac{i}{8}\int (Z_u\Psi_q - Z_q\Psi_u)\hat{G}\overline{(Z_u\Psi_q - Z_q\Psi_u)}\, du\, dq \\ & + \frac{i}{16}\int \Big\{ \left[(Z_u\Psi_q - Z_q\Psi_u)^2/Z_u\right]\; \hat{E}\overline{(Z-u)} \\ & \qquad -(Z-u)\,\hat{E}\overline{[(Z_u\Psi_q - Z_q\Psi_u)^2/Z_u]}\Big\}\, du\, dq. \end{aligned} \tag{13}$$

$$\Psi \equiv (1 + i\hat{H})\psi$$

$$G(k,m) = \frac{-2i}{\sqrt{k^2+m^2}+|k|}, \tag{14}$$

$$E(k,m) = \frac{2|k|}{\sqrt{k^2+m^2}+|k|}. \tag{15}$$

3. Variational derivatives

$$\frac{\delta\tilde{\mathcal{K}}}{\delta\psi} = -\hat{H}\psi_u + 2\,\mathsf{Re}\,\left[(1-i\hat{H})\frac{\delta\tilde{\mathcal{F}}}{\delta\Psi}\right], \tag{16}$$

$$\begin{aligned}\frac{\delta\tilde{\mathcal{F}}}{\delta\Psi} &= \frac{i}{8}Z_q\hat{\partial}_u[\hat{G}\overline{(Z_u\Psi_q - Z_q\Psi_u)} + (\Psi_q - Z_q\Psi_u/Z_u)\hat{E}\overline{(Z-u)}] \\ &\quad -\frac{i}{8}\,Z_u\,\hat{\partial}_q[\hat{G}\overline{(Z_u\Psi_q - Z_q\Psi_u)} + (\Psi_q - Z_q\Psi_u/Z_u)\hat{E}\overline{(Z-u)}],\end{aligned} \tag{17}$$

$$\begin{aligned}\frac{\delta\tilde{\mathcal{F}}}{\delta Z} &= -\frac{i}{8}\Psi_q\hat{\partial}_u[\hat{G}\overline{(Z_u\Psi_q - Z_q\Psi_u)} + (\Psi_q - Z_q\Psi_u/Z_u)\hat{E}\overline{(Z-u)}] \\ &\quad +\frac{i}{8}\,\Psi_u\,\hat{\partial}_q[\hat{G}\overline{(Z_u\Psi_q - Z_q\Psi_u)} + (\Psi_q - Z_q\Psi_u/Z_u)\hat{E}\overline{(Z-u)}] \\ &\quad +\frac{i}{16}\,[\hat{\partial}_u[(\Psi_q - Z_q\Psi_u/Z_u)^2\hat{E}\overline{(Z-u)}] - \hat{E}\overline{(\Psi_q - Z_q\Psi_u/Z_u)^2 Z_u}].\end{aligned} \tag{18}$$

III. Numerical experiments

1. Example of evolution of a perturbed giant breather in 2D.

2. Example of evolution of a perturbed high-amplitude oblique soliton into a zigzag structure

3-4. Two small sets of typical numerical experiments designated as A1-A4 and B1-B3. Within each set, at $t = 0$ the normal Fourier modes of the wave field were taken in the form $a_{km}(0) = cF(k, m)\exp(i\gamma_{km})$, with a positive function $F(k, m)$ having two nearly Gaussian maxima at $\mathbf{k}_0 \pm \Delta\mathbf{k}/2$, and with quasi-random initial phases γ_{km}, different for A and for B. In each experiment a choice of the coefficient c gave different values of the total energy $E_{A1}, E_{A2}, E_{A3}, E_{A4}$ and E_{B1}, E_{B2}, E_{B3}. In set A we took $\mathbf{k}_0 = (40.0, -2.5)$ and $\Delta\mathbf{k} = (7.0, 2.0)$, so a case $\theta < \theta_*$ was simulated, while in set B it was a crossing sea state with $\theta = \pi/2$: $\mathbf{k}_0 \pm \Delta\mathbf{k}/2 = (39.5, \pm 3.5)$.

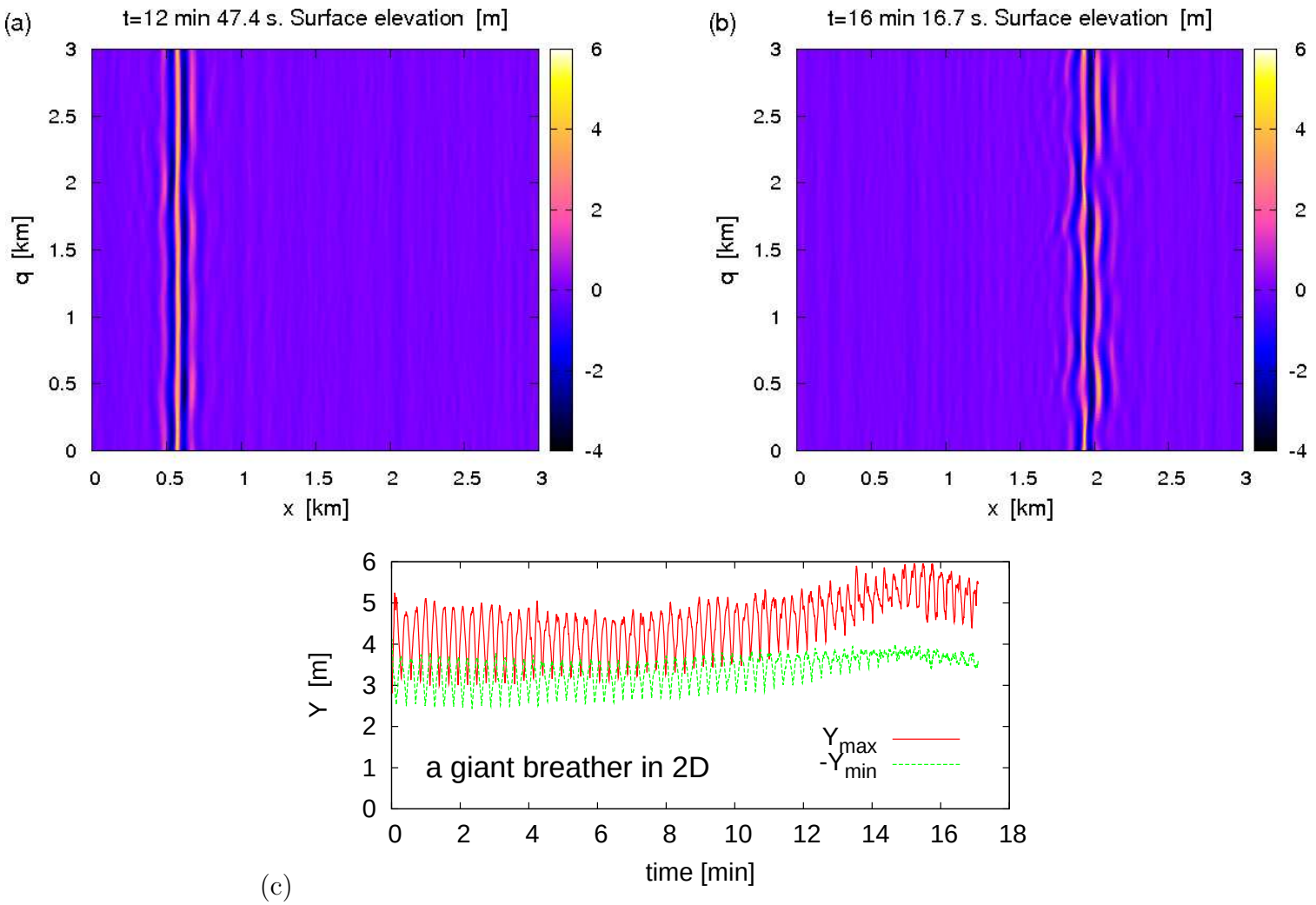

Figure 2: (a)-(b): Evolution of a perturbed giant breather in 2D; (c) Maximum and minimum elevation of the giant breather vs. time.

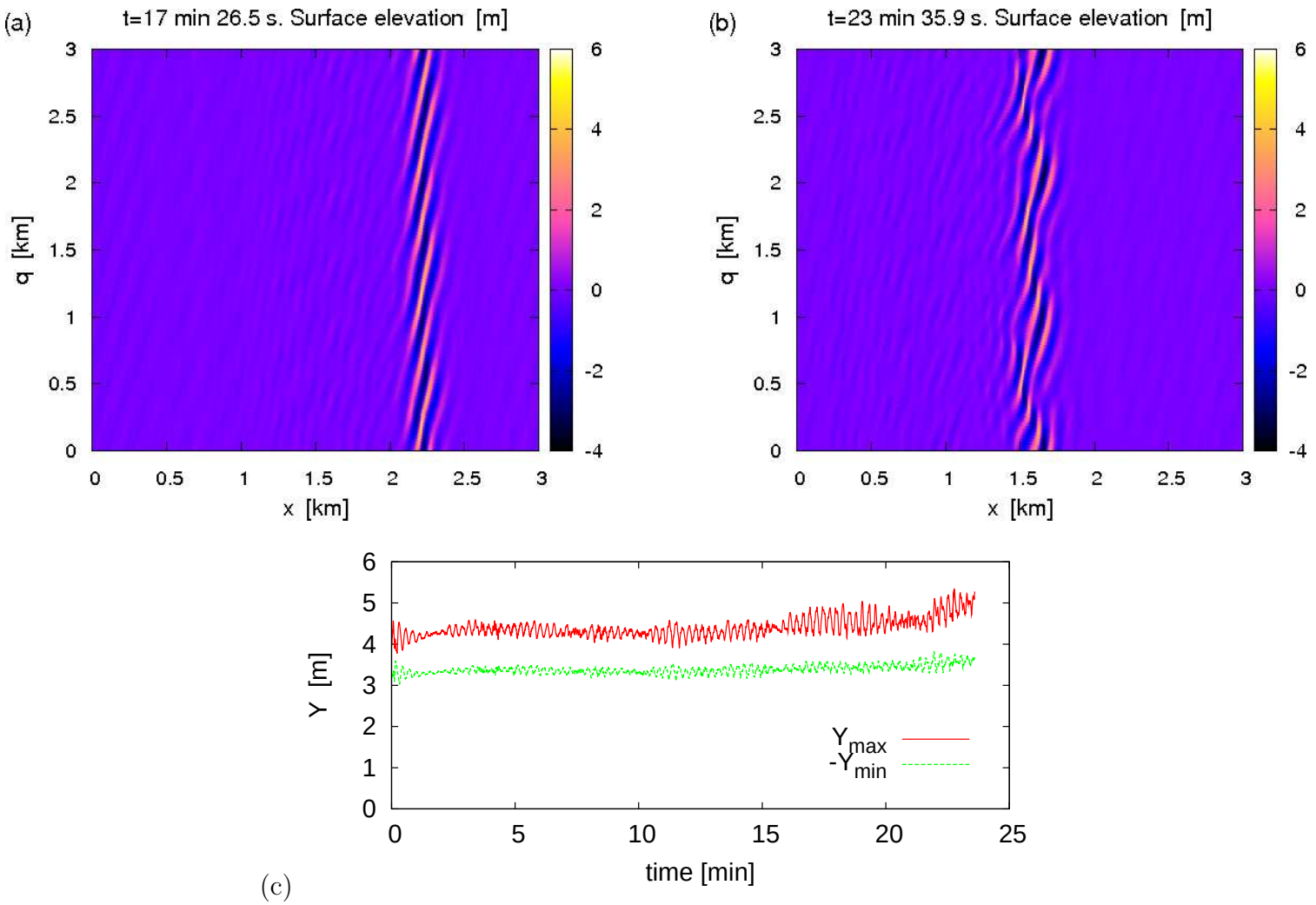

Figure 3: (a)-(b): Evolution of a perturbed high-amplitude oblique soliton into a zigzag structure; (c) Maximum and minimum elevation of the oblique soliton vs. time.

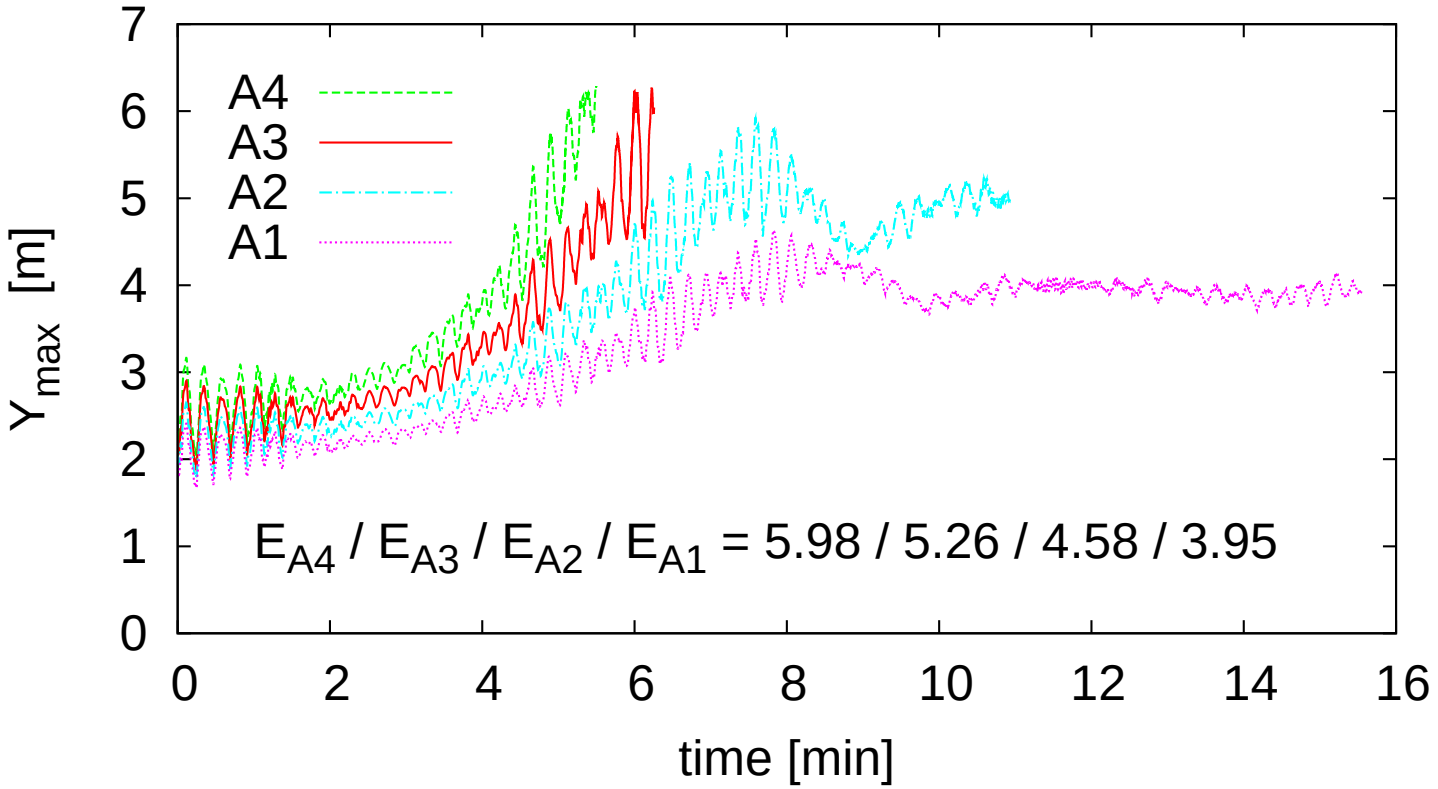

Figure 4: Maximum elevation of the free surface vs. time in the numerical experiments A1-A4.

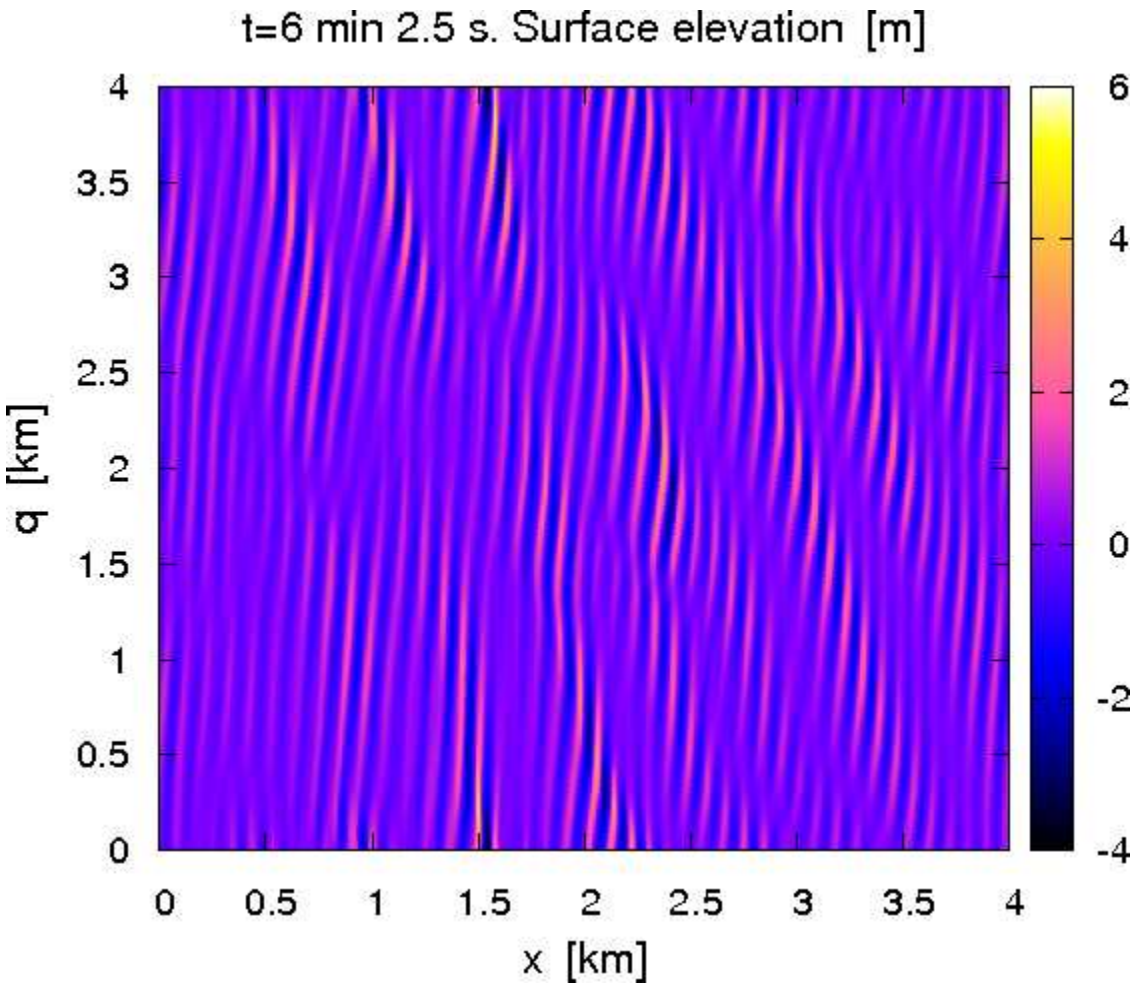

Figure 5: Experiment A3: the two big waves are at $x \approx 1.6$ km, $q \approx [3.7 \cdots 3.9]$ km, and at $x \approx 1.5$ km, $q \approx [0.1 \cdots 0.3]$ km.

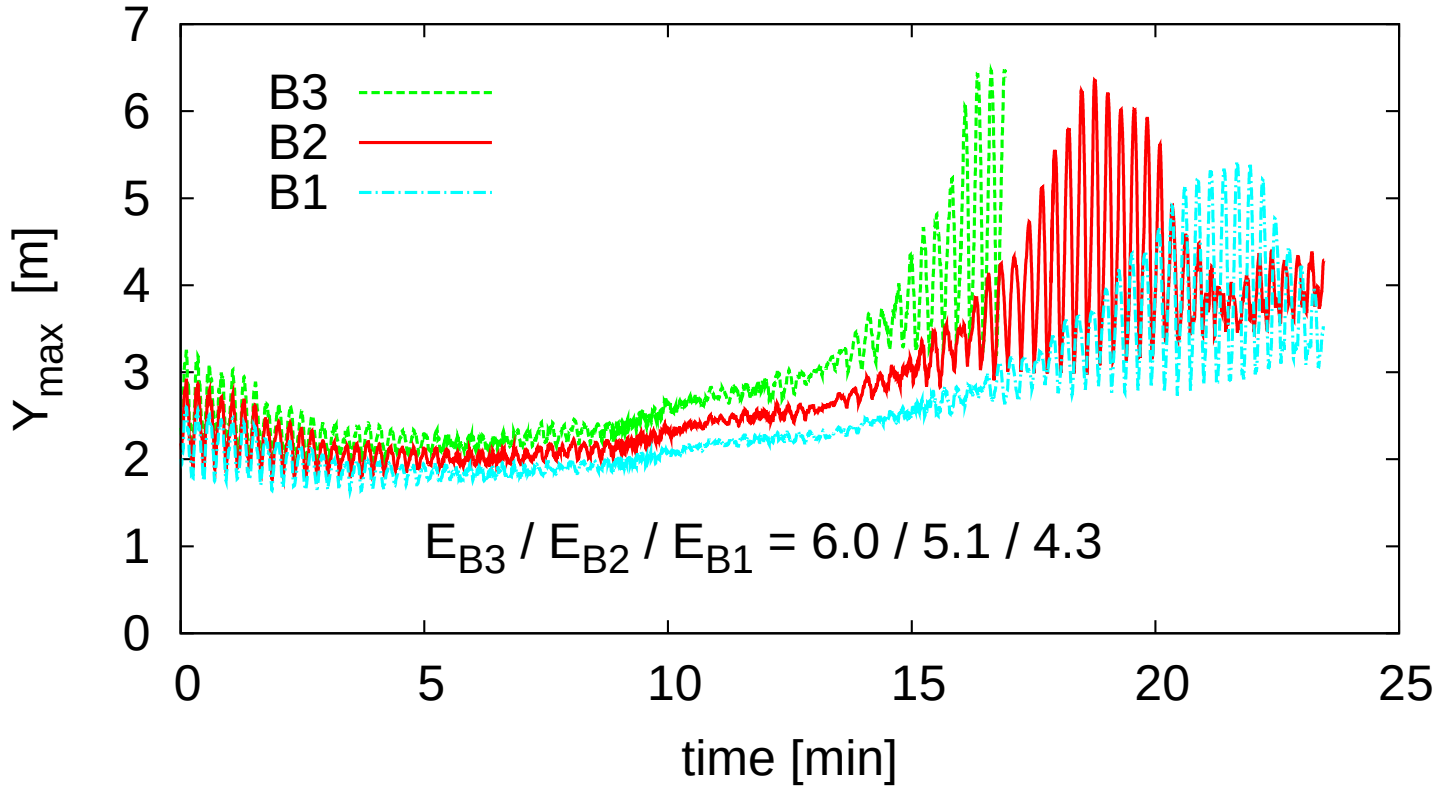

Figure 6: Maximum elevation of the free surface in the numerical experiments B1-B3.

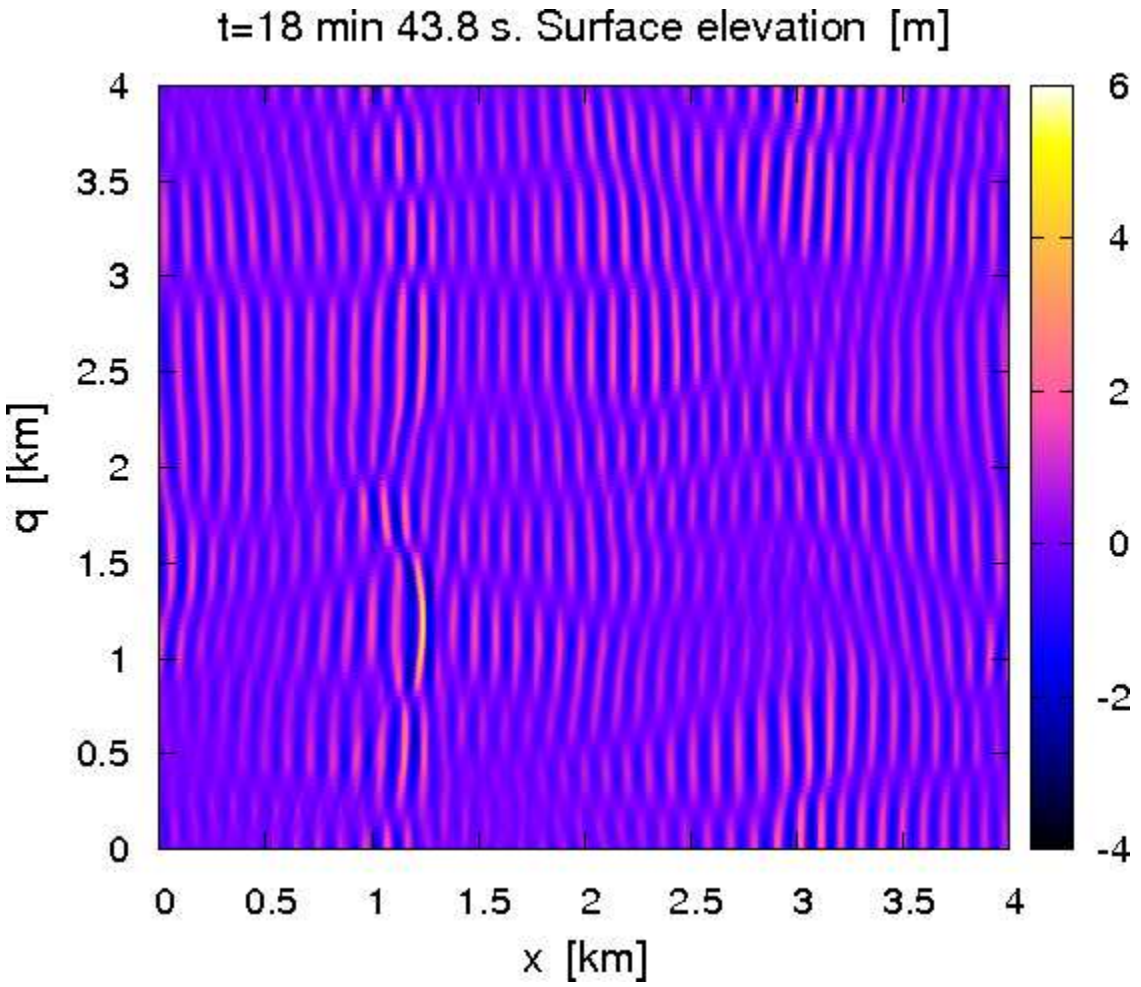

Figure 7: Experiment B2: the rogue wave is at $x \approx 1.2$ km, $q \approx [1.0 \cdots 1.3]$ km.

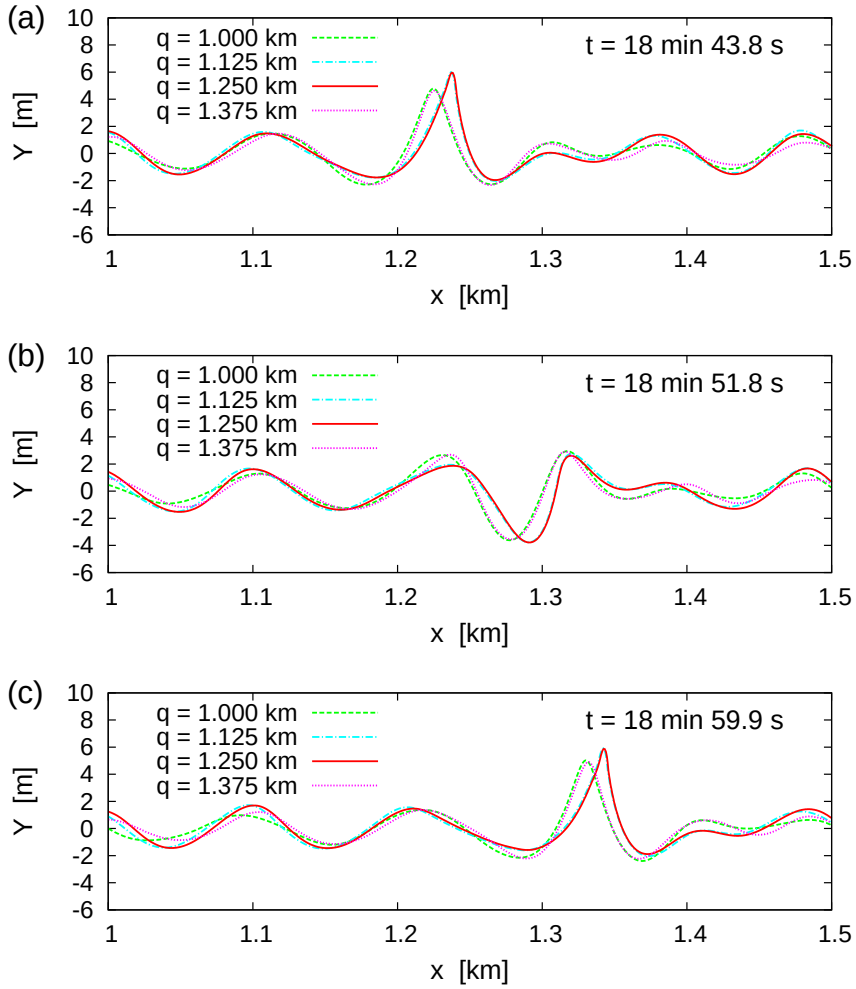

Figure 8: (a) profiles of the freak wave from Fig.7; (b) 8 s later: "a hole in the sea"; (c) 16 s later: the big wave has risen again.